International Journal of Heat and Mass Transfer 84 (2015) 809–820

Contents lists available at ScienceDirect

International Journal of Heat and Mass Transfer

journal homepage: www.elsevier.com/locate/ijhmt

On the utilization of the mean beam length concept in the evaluation of radiative heat transfer in isothermal three-dimensional non-gray system

Walter W. Yuen

Department of Mechanical Engineering, University of California at Santa Barbara, Santa Barbara, California 93105, United States

ARTICLE INFO

Article history:
Received 23 November 2014
Accepted 14 January 2015

Keywords:
Mean beam length
Radiative heat transfer
Non-gray mixture
RAD-NNET
MBL-NNET

ABSTRACT

The mean beam length concept, which is defined traditionally for the evaluation of emission of a gas volume to its surrounding boundary, is generalized to apply to three-dimensional surface–surface and volume–surface radiative exchange with an intervening non-gray $N_2/CO_2/H_2O$/soot mixture at one atmosphere. The concept is demonstrated to be effective in providing a simple, efficient and accurate approach to compute radiative heat transfer in non-gray three-dimensional mixtures. Using numerical data generated for a rectangular enclosure, the mean beam lengths are shown to depend mainly on the total partial pressure of the absorbing gas and soot volume fraction. The mean beam length's dependence on the mixture temperature and the fractional proportion of the individual gaseous specie does not have a strong influence on the mixture total absorptance and emittance. The Hottel's constant mean beam length approach is shown to be accurate only in the prediction of the emittance of a non-luminous mixture (i.e. without soot). For the mixture absorptance and the emittance/absorptance of a luminous mixture, the Hottel's approach is generally inaccurate. A neural network, MBL-NNET, is developed to correlate the mean beam length data for the mixture in the enclosure. The two neural networks (MBL-NNET and RAD-NNET) are shown to be an effective approach in the evaluation of radiation heat transfer in practical engineering systems.

1. Introduction

Over the years, the use of a constant mean beam length to characterize radiative heat transfer in three-dimensional system is a common practice in the engineering community because of the mathematical complexity of three-dimensional non-gray radiative heat transfer. The concept was first introduced by Hottel [1] and many researchers [2–6] in the 1960 and 1970's have contributed to the further development of this concept. Focusing largely on gaseous absorption bands, analytical expressions for the mean beam length at different optical limits and geometrical configurations were determined [3–5]. In general, mean beam length was observed not to be a constant and depend strongly on the behavior of the absorption bands, gas temperature and pressure and the enclosure geometry.

For the last thirty years, only a few works [7–9] have been reported to improve the understanding of the mean beam length concept. These works, however, were focused largely on the extension of the mean beam length concept to a scattering medium. In general, the concept of mean beam length has not received much attention as the research community devoted much of its effort in the development of solution methods which can compute directly the numerical solution for three-dimensional non-gray radiative heat transfer. These efforts have led to significant progress in the understanding of the mathematics of radiation heat transfer and many highly sophisticated solution methods were developed (e.g. the differential method [10], flux method [11], zonal method [12], finite volume method [13], discrete ordinate method [14], Monte Carlo [15] and the weighted-sum-of-gray-gas model [16]). Some of them have been implemented in commercial CFD codes (e.g. the finite volume method in FDS [17] and the weight-sum-of-gray-gas model and discrete coordinate method in FLUENT [18]).

For the practicing engineering community, however, all of these methods still have the issue of uncertain accuracy and complexity of implementation for general three-dimensional non-gray systems. Currently, for example, there has been no published study and comparison of benchmark solution which demonstrate readily the relative accuracy of these methods for the evaluation of radiative heat transfer in a three-dimensional non-gray medium. Indeed, in all of the existing undergraduate heat transfer textbooks (for example, Refs. [19,20]) and radiation text books (for example

http://dx.doi.org/10.1016/j.ijheatmasstransfer.2015.01.080
0017-9310/

Nomenclature

a_λ	absorption coefficient
$a_{s\lambda}$	absorption coefficient of soot, Eq. (14)
a_i^k	neural network parameters, k = 1, 2, 3
A_i	area element i (i = 1, 6), Fig. 1
b_i^k	neural network parameters, k = 1, 2, 3
C_{CO_2}	correlation constant in Hottel's MBL correlation, Eq. (23b)
C_{H_2O}	correlation constant in Hottel's MBL correlation, Eq. (23a)
$e_{\lambda b}$	Planck function
F_{ij}	view factor between A_i and A_j
F_{CO_2}	fraction of CO_2, Eq. (5)
P_g	partial pressure of absorbing gas (kPa), Eq. (4)
L	the line-of-sight distance between the two integration area elements dA_i and dA_j, Eq. (1)
$L_{ma,ij}$	mean beam length for the total geometric mean absorptance between two areas A_i and A_j, Eq. (7)
$L_{me,ij}$	mean beam length for the total geometric mean emittance between two areas A_i and A_j, Eq. (8)
$L_{ma,i}$	mean beam length for the total geometric mean absorptance between the mixture volume and area A_i, Eq. (10)
$L_{me,i}$	mean beam length for the total geometric mean absorptance between the mixture volume and area A_i, Eq. (11)
P_{H_2O}	partial pressure of H_2O (kPa)
P_{CO_2}	partial pressure of CO_2 (kPa)
S_iS_j	surface–surface exchange factor between A_i and A_j.
T	temperature (K)
T_w	wall temperature (K)
T_g	mixture temperature (K)
W_{ij}^k	neural network parameters, k = 1, 2, 3
X	dimension of rectangular enclosure, Fig. 1
Y	dimension of rectangular enclosure, Fig. 1
Z	dimension of rectangular enclosure, Fig. 1
α_{ij}	total geometric mean absorptance by the medium between two areas, A_i and A_j, Eq. (7)
α_i	total geometric mean absorptance due to the total absorption of the energy radiated from one of its bounding areas, A_i, by the full volume of the mixture, Eq. (9)
ε_{ij}	total geometric mean emittance by the medium between two areas, A_i and A_j, Eq. (8)
ε_i	total geometric mean emittance by the full volume of the medium to area A_i, Eq. (11)
ε_{1d}	one-dimensional total geometric emittance of the mixture
σ	Stefan Boltzmann constant
τ_{1d}	one-dimensional total transmittance through the mixture, Eq. (3)
τ_{ij}	total geometric mean transmittance between two areas, A_i and A_j.
$\Delta\alpha$	correlation parameter in Hottel's MBL correlation
$\Delta\varepsilon$	correlation parameter in Hottel's MBL correlation

Refs. [21,22]), the Hottel's constant mean beam length approach and the Hottel's emittance chart [1] is still the recommended approach to determine the emittance and absorptance of a three-dimensional non-gray combustion gases. There is no recommended approach for a luminous gas mixture with soot. In general, it appears that the research on solution methods over the past thirty years have made very little impact on furthering the capability to evaluate radiative heat transfer in the practical engineering community.

In this work, a systematic approach is presented to demonstrate that the mean beam length concept can be used to provide a simple, efficient and accurate approach for practicing engineers to account for the effect of radiative heat transfer for a non-gray mixture in a three-dimensional enclosure. This approach is illustrated specifically for the evaluation of radiative heat transfer in a rectangular enclosure with a non-gray $N_2/CO_2/H_2O$/soot mixture at one atmosphere. In Section 2, the mathematical formulation and solution procedure are presented. Utilizing RAD-NNET [23], which is a neural network correlation of the one-dimensional narrow-band model RADCAL [24], the total radiative exchange factors for surface–surface and volume–surface are generated by direct numerical integration. Mean beam lengths for total radiative exchange are then generated. As shown in reference [23], RAD-NNET is a neural network correlation of the RADCAL narrow-band model [24] with a relative error in the total absorptance of less than 5% over all ranges of the mixture properties (except when the total absorptance is less than 0.01, at which the RAD-NETT prediction has a relative error of less than 100%). The numerical solutions for the surface–surface and volume-service radiative exchange and the associated mean beam length can thus be considered as identical to those generated directly with RADCAL, within the 5% accuracy. Numerical solutions for the total geometric mean absorptance and emittance are presented for the considered geometry and mixture as benchmark solutions. In Section 3, the mean beam lengths are generated and the accuracy of the Hottel's mean beam length in determining the total geometric mean absorptance and emittance is assessed. A neural network, MBL-NNET, is further generated to correlate the mean beam lengths for total radiative exchange. Together with RAD-NNET, the two neural network approach is shown to be an efficient and accurate approach in determining the mixture's emittance and absorptance.

2. Mathematical formulation

The solution approach is developed for a rectangular enclosure with dimensions X, Y and Z is shown in Fig. 1. For a medium with uniform absorption coefficient, a_λ, the surface–surface total geometric mean transmittance between two areas, A_i and A_j, is given by

$$\tau_{ij} = \frac{S_iS_j}{A_iF_{ij}} = \frac{1}{A_iF_{ij}\sigma T_w^4}\int_0^\infty \int_{A_i}\int_{A_j} \frac{e_{\lambda b}(T_w)e^{-a_\lambda L}\cos\theta_i\cos\theta_j}{\pi L^2} dA_i dA_j d\lambda \tag{1}$$

where L is the line-of-sight distance between the two integration area elements dA_i and dA_j. θ_i and θ_j are the angles between the

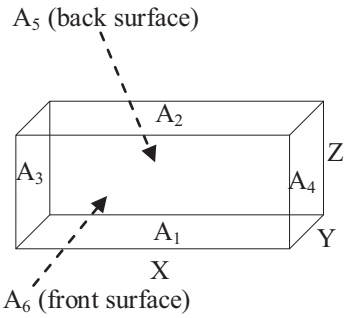

Fig. 1. The geometry and area identification of the rectangular enclosure.

Table 1a
Geometric mean emittance for a mixture with $F_{CO_2} = 0.0$, $f_v = 0.0$.

T_g (K)	P_gX (kPa m)	ε_{12}	ε_{13}	ε_{15}	ε_1
	1	5.395E−02	3.986E−02	3.772E−02	4.367E−02
300	10	1.390E−01	1.052E−01	1.057E−01	1.160E−01
	100	2.812E−01	2.351E−01	2.352E−01	2.497E−01
	1	3.208E−02	2.230E−02	2.039E−02	2.482E−02
1000	10	1.402E−01	9.677E−02	9.715E−02	1.106E−01
	100	4.087E−01	3.098E−01	3.113E−01	3.416E−01
	1	1.802E−02	1.325E−02	1.126E−02	1.416E−02
1500	10	1.094E−01	7.231E−02	7.093E−02	8.363E−02
	100	3.715E−01	2.707E−01	2.736E−01	3.035E−01
	1	1.041E−02	8.752E−03	6.683E−03	8.652E−03
2000	10	7.849E−02	5.076E−02	4.936E−02	5.911E−02
	100	3.186E−01	2.241E−01	2.268E−01	2.548E−01

Table 1b
Geometric mean emittance for a mixture with $F_{CO_2} = 0.8$, $f_v = 0.0$.

T_g (K)	P_gX (kPa-m)	ε_{12}	ε_{13}	ε_{15}	ε_1
	1	6.645E−02	4.763E−02	4.561E−02	5.297E−02
300	10	1.722E−01	1.294E−01	1.304E−01	1.432E−01
	100	3.380E−01	2.764E−01	2.769E−01	2.960E−01
	1	5.800E−02	4.325E−02	4.112E−02	4.727E−02
1000	10	1.475E−01	1.100E−01	1.109E−01	1.221E−01
	100	3.334E−01	2.611E−01	2.620E−01	2.843E−01
	1	3.934E−02	2.895E−02	2.687E−02	3.161E−02
1500	10	1.111E−01	8.146E−02	8.170E−02	9.091E−02
	100	2.844E−01	2.163E−01	2.185E−01	2.385E−01
	1	2.407E−02	1.807E−02	1.600E−02	1.934E−02
2000	10	7.668E−02	5.637E−02	5.436E−02	6.219E−02
	100	2.118E−01	1.579E−01	1.598E−01	1.756E−01

Table 1c
Geometric mean emittance for a mixture with $F_{CO_2} = 1.0$, $f_v = 0.0$.

T_g (K)	P_gX (kPa m)	ε_{12}	ε_{13}	ε_{15}	ε_1
	1	4.795E−02	3.591E−02	3.376E−02	3.907E−02
300	10	1.055E−01	8.404E−02	8.401E−02	9.081E−02
	100	1.663E−01	1.425E−01	1.436E−01	1.504E−01
	1	5.344E−02	4.158E−02	3.929E−02	4.464E−02
1000	10	1.051E−01	8.391E−02	8.407E−02	9.066E−02
	100	1.700E−01	1.449E−01	1.460E−01	1.532E−01
	1	3.881E−02	2.945E−02	2.729E−02	3.176E−02
1500	10	8.794E−02	6.820E−02	6.802E−02	7.439E−02
	100	1.651E−01	1.346E−01	1.376E−01	1.452E−01
	1	2.463E−02	1.879E−02	1.668E−02	2.000E−02
2000	10	6.352E−02	4.907E−02	4.681E−02	5.296E−02
	100	1.311E−01	1.058E−01	1.061E−01	1.139E−01

Table 2a
Geometric mean absorptance for a mixture with $F_{CO_2} = 0.0$, $f_v = 0.0$ with $T_w = 1000$ K.

T_g (K)	P_gX (kPa-m)	α_{12}	α_{13}	α_{15}	α_1
	1	3.027E−02	2.285E−02	2.074E−02	2.456E−02
300	10	9.673E−02	7.094E−02	7.067E−02	7.901E−02
	100	2.612E−01	2.042E−01	2.058E−01	2.227E−01
	1	3.208E−02	2.230E−02	2.039E−02	2.482E−02
1000	10	1.402E−01	9.677E−02	9.715E−02	1.106E−01
	100	4.087E−01	3.098E−01	3.113E−01	3.416E−01
	1	3.042E−02	2.074E−02	1.888E−02	2.324E−02
1500	10	1.655E−01	1.097E−01	1.104E−01	1.276E−01
	100	4.887E−01	3.683E−01	3.701E−01	4.069E−01
	1	2.767E−02	1.896E−02	1.711E−02	2.116E−02
2000	10	1.732E−01	1.119E−01	1.129E−01	1.316E−01
	100	5.457E−01	4.060E−01	4.083E−01	4.509E−01

line-of-sight and the unit normal vector of the two differential area elements and F_{ij} is the view factor between the two areas. The spectral integration can be carried out after the selection of a particular

Table 2b
Geometric mean absorptance for a mixture with $F_{CO_2} = 0.8$, $f_v = 0.0$ with $T_w = 1000$ K.

T_g (K)	P_gX (kPa m)	α_{12}	α_{13}	α_{15}	α_1
	1	4.607E−02	3.648E−02	3.418E−02	3.882E−02
300	10	1.003E−01	7.884E−02	7.885E−02	8.562E−02
	100	2.087E−01	1.657E−01	1.671E−01	1.798E−01
	1	5.800E−02	4.325E−02	4.112E−02	4.727E−02
1000	10	1.475E−01	1.100E−01	1.109E−01	1.221E−01
	100	3.334E−01	2.611E−01	2.620E−01	2.843E−01
	1	6.158E−02	4.361E−02	4.163E−02	4.869E−02
1500	10	1.664E−01	1.223E−01	1.234E−01	1.366E−01
	100	3.952E−01	3.056E−01	3.067E−01	3.343E−01
	1	6.092E−02	4.155E−02	3.972E−02	4.713E−02
2000	10	1.751E−01	1.283E−01	1.294E−01	1.434E−01
	100	4.337E−01	3.302E−01	3.330E−01	3.638E−01

Table 2c
Geometric mean absorptance for a mixture with $F_{CO_2} = 1.0$, $f_v = 0.0$ with $T_w = 1000$ K.

T_g (K)	P_gX (kPa m)	α_{12}	α_{13}	α_{15}	α_1
	1	3.672E−02	3.100E−02	2.860E−02	3.208E−02
300	10	6.236E−02	5.283E−02	5.227E−02	5.567E−02
	100	9.236E−02	7.962E−02	7.980E−02	8.370E−02
	1	5.344E−02	4.158E−02	3.929E−02	4.464E−02
1000	10	1.051E−01	8.391E−02	8.407E−02	9.066E−02
	100	1.700E−01	1.449E−01	1.460E−01	1.532E−01
	1	5.959E−02	4.386E−02	4.176E−02	4.820E−02
1500	10	1.265E−01	9.904E−02	9.949E−02	1.079E−01
	100	2.183E−01	1.824E−01	1.839E−01	1.942E−01
	1	6.187E−02	4.335E−02	4.139E−02	4.862E−02
2000	10	1.403E−01	1.088E−01	1.093E−01	1.189E−01
	100	2.502E−01	2.094E−01	2.093E−01	2.223E−01

Table 3a
Geometric total mean emittance for a gas/soot mixture with $F_{CO_2} = 0.8$.

T_g (K)	f_vX (m)	$P_gX = 0$	1 kPa m	10 kPa m	100 kPa m
	1.000E−08	3.403E−03	5.619E−02	1.462E−01	2.985E−01
300	1.000E−07	3.389E−02	8.511E−02	1.724E−01	3.210E−01
	3.000E−07	9.682E−02	1.450E−01	2.262E−01	3.675E−01
	1.000E−08	1.135E−02	5.809E−02	1.322E−01	2.925E−01
1000	1.000E−07	1.067E−01	1.490E−01	2.163E−01	3.620E−01
	3.000E−07	2.718E−01	3.061E−01	3.607E−01	4.807E−01
	1.000E−08	1.702E−02	4.824E−02	1.067E−01	2.522E−01
1500	1.000E−07	1.535E−01	1.815E−01	2.333E−01	3.607E−01
	3.000E−07	3.655E−01	3.878E−01	4.280E−01	5.255E−01
	1.000E−08	2.269E−02	4.177E−02	8.394E−02	1.954E−01
2000	1.000E−07	1.964E−01	2.133E−01	2.500E−01	3.452E−01
	3.000E−07	4.403E−01	4.536E−01	4.816E−01	5.506E−01

spectral model characterizing the mixture's absorption characteristics (e.g. RADCAL [24]). For a mixture of N_2, CO_2, H_2O and soot, Eq. (1) can be written as

$$\tau_{ij} = \frac{S_i S_j}{A_i F_{ij}} = \frac{1}{A_i F_{ij}} \int_{A_i} \int_{A_j} \frac{\tau_{1d}(P_g L, F_{CO_2}, f_v L, T_w, T_g) \cos\theta_i \cos\theta_j}{\pi L^2} dA_i dA_j \quad (2)$$

where τ_{1d} is the one-dimensional total transmittance through the mixture given by

$$\tau_{1d}(P_g L, F_{CO_2}, f_v L, T_w, T_g) = \frac{1}{\sigma T_w^4} \int_0^\infty e_{\lambda b}(T_w) e^{-a_\lambda L} d\lambda \quad (3)$$

and can be evaluated with a spectral model such as RADCAL [24]. In Eq. (3), T_w is the temperature of the emitting wall, T_g the mixture's temperature and f_v the soot volume fraction. P_g is the total partial pressure of the absorbing gas given by

$$P_g = P_{H_2O} + P_{CO_2} \quad (4)$$

and

$$F_{CO_2} = \frac{P_{CO_2}}{P_{H_2O} + P_{CO_2}} \tag{5}$$

with P_{CO_2} and P_{H_2O} being the partial pressure of CO_2 and H_2O respectively. In analogy to the Hottel's definition of mean beam length, a surface–surface mean beam length, $L_{m,ij}$, is defined to be the length scale such that the one-dimensional total transmittance is equivalent to the total geometric mean transmittance, i.e.

Table 3b
Geometric total mean absorptance for a gas/soot mixture with $F_{CO_2} = 0.8$.

T_g (K)	f_vX (m)	$P_gX = 0$	1 kPa m	10 kPa m	100 kPa m
	1.E−08	1.135E−02	4.973E−02	9.598E−02	1.891E−01
300	1.E−07	1.067E−01	1.413E−01	1.831E−01	2.673E−01
	3.E−07	2.718E−01	2.998E−01	3.337E−01	4.006E−01
	1.E−08	1.135E−02	5.809E−02	1.322E−01	2.925E−01
1000	1.E−07	1.067E−01	1.490E−01	2.163E−01	3.620E−01
	3.E−07	2.718E−01	3.061E−01	3.607E−01	4.807E−01
	1.E−08	1.135E−02	5.949E−02	1.464E−01	3.420E−01
1500	1.E−07	1.067E−01	1.501E−01	2.294E−01	4.073E−01
	3.E−07	2.718E−01	3.067E−01	3.725E−01	5.188E−01
	1.E−08	1.135E−02	5.794E−02	1.532E−01	3.711E−01
2000	1.E−07	1.067E−01	1.488E−01	2.358E−01	4.326E−01
	3.E−07	2.718E−01	3.058E−01	3.779E−01	5.385E−01

$$\tau_{ij} = \tau_{1d}\left(P_g L_{m,ij}, F_{CO_2}, f_v L_{m,ij}, T_w, T_g\right) \tag{6}$$

The corresponding surface–surface total geometric mean absorptance due to the medium bounded by the two surface A_i and A_j, radiating in the direction of A_i, is given by

$$\alpha_{ij} = 1 - \tau_{ij} = 1 - \tau_{1d}\left(P_g L_{ma,ij}, F_{CO_2}, f_v L_{ma,ij}, T_w, T_g\right) \tag{7}$$

When the emission temperature T_w is identical to the mixture temperature, the surface–surface total geometric mean absorptance is equivalent to the surface–surface total geometric emittance which is

$$\varepsilon_{ij} = 1 - \tau_{ij} = 1 - \tau_{1d}\left(P_g L_{me,ij}, F_{CO_2}, f_v L_{me,ij}, T_g, T_g\right) \tag{8}$$

For application, it is important to evaluate the total absorption of the energy radiated from one of its bounding areas, A_i, by the full volume of the mixture. This leads to the definition of a surface–volume total geometric mean absorptance given by

$$\alpha_i = \frac{1}{A_i \sigma T_w^4} \sum_j \int_0^\infty \int_{A_i} \int_{A_j} \frac{e_{\lambda b}(T_w)\left(1 - e^{-a_\lambda L}\right) \cos\theta_i \cos\theta_j}{\pi L^2} dA_i dA_j d\lambda$$
$$= 1 - \sum_j F_{ij} \tau_{ij} \tag{9}$$

A surface–volume absorption mean beam length, corresponding to surface A_i, can be introduced as

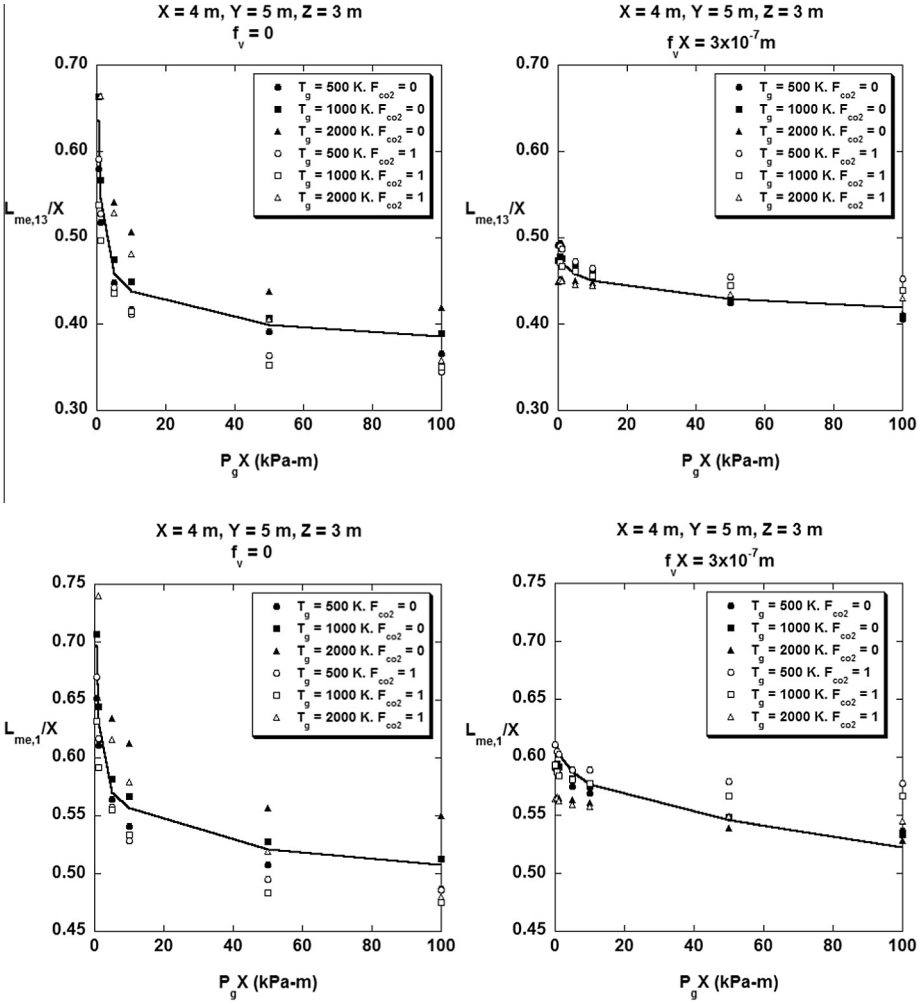

Fig. 2a. Mean beam lengths for geometric mean emittance at different total absorption pressure pathlength (P_gX) and soot volume fraction pathlength (f_vX). The solid line is the mean beam length averaged over the mixture temperature (T_g) and composition (F_{CO_2}).

$$\alpha_i = 1 - \tau_{1d}\left(P_g L_{ma,i}, F_{CO_2}, f_v L_{ma,i}, T_w, T_g\right) \tag{10}$$

Similarly, a surface–volume emission mean beam length, characterizing the absorption of the total emission from the mixture by the surface A_i, can be written as

$$\varepsilon_i = 1 - \tau_{1d}\left(P_g L_{me,i}, F_{CO_2}, f_v L_{me,i}, T_g, T_g\right) \tag{11}$$

The two surface–volume mean beam lengths are related to the six surface–surface mean beam lengths by the relations

$$\tau_{1d}\left(P_g L_{ma,i}, F_{CO_2}, f_v L_{ma,i}, T_w, T_g\right) = \sum_{j=1}^{6} F_{ij}\,\tau_{1d}\left(P_g L_{ma,ij}, F_{CO_2}, f_v L_{ma,ij}, T_w, T_g\right) \tag{12}$$

$$\tau_{1d}\left(P_g L_{me,i}, F_{CO_2}, f_v L_{me,i}, T_g, T_g\right) = \sum_{j=1}^{6} F_{ij}\,\tau_{1d}\left(P_g L_{me,ij}, F_{CO_2}, f_v L_{me,ij}, T_g, T_g\right) \tag{13}$$

It should be noted that a direct numerical integration, utilizing a spectral model such as RADCAL, is quite time consuming and impractical in an actual engineering design calculations in which the pressure, temperature and the concentration of the different gaseous species and soot can be changing continuously. In the present work, all the numerical integrations will be evaluated efficiently using RAD-NNET. The numerical data thus have the same degree of accuracy as RAD-NNET (which has a relative error of less than 5% when the absorptance or emittance is greater than 0.01 and a relative error of less than 100% otherwise). Numerical data generated for different mixture conditions for a non-luminous gas mixture ($f_v = 0$) are presented in Tables 1a–2c The mathematical behavior for ε_{15} and α_{15} are generally similar to that of ε_{13} and α_{13} Data for ε_{15} and α_{15} are thus not presented in Tables 1a, 1b, 2a and 2b to avoid making the table excessively large. Data for a luminous mixture ($f_v > 0$) are presented in Tables 3a and 3b. As in RADCAL, the soot absorption characteristics are assumed to be that of the Rayleigh small particle limit given by

$$a_{\lambda s}(f_v) = \frac{c}{\lambda} \tag{14}$$

with

$$c = 36\pi f_v \frac{n\kappa}{\left(n^2 - \kappa^2 + 2\right)^2 + 4n^2\kappa^2} \tag{15}$$

where n and κ are the real and imaginary component of the soot's index of refraction respectively. Note that the numerical data presented in these tables are selected to cover the range of the mixture data which will demonstrate the effect of the overlapping of absorption bands of CO_2 and H_2O as well as simultaneous effect of soot and gas absorption. These data can be used as effective benchmark solutions to demonstrate the relative accuracy of the different solution methods.

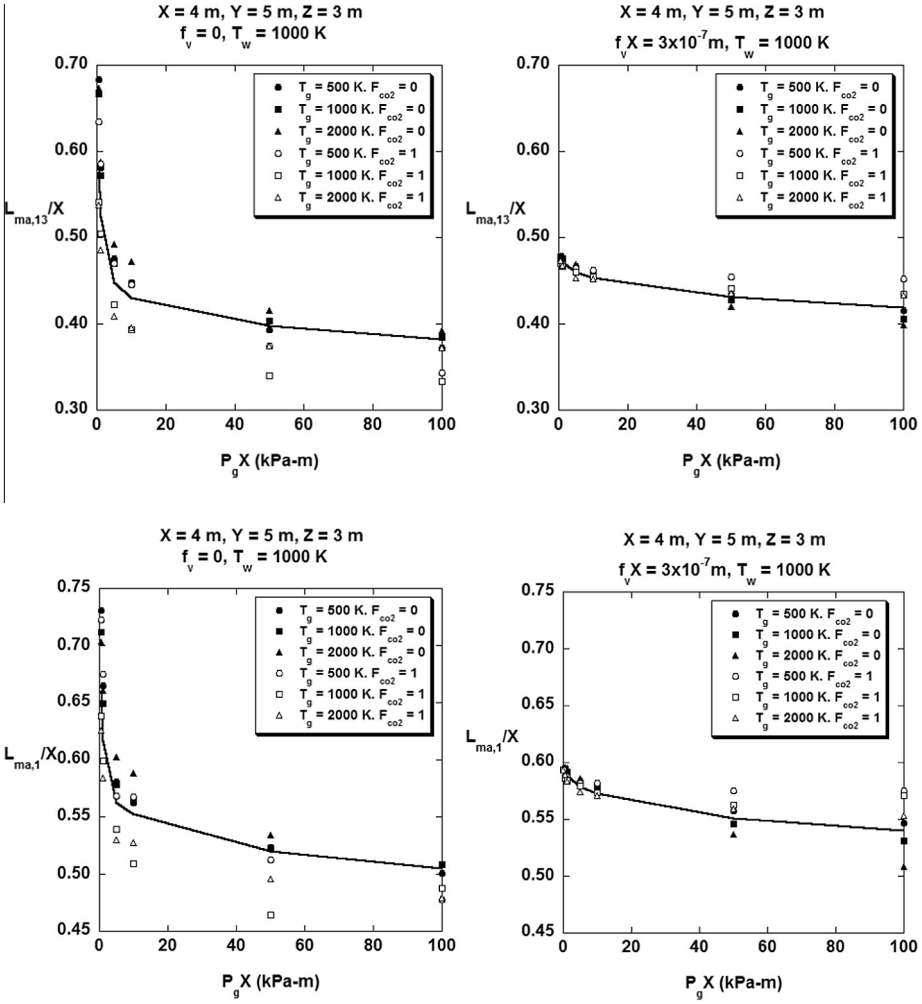

Fig. 2b. Mean beam lengths for geometric mean absorptance at different total absorption pressure pathlength (P_gX) and soot volume fraction pathlength (f_vX). The solid line is the mean beam length averaged over the mixture temperature (T_g) and composition (F_{CO_2}).

3. Results and discussion

3.1. The mean beam lengths

Based on numerical solution and RAD-NNET and Eqs. 7, 8, 10 and 11, the absorption mean beam length and emission mean beam length for both surface–surface exchange and volume–surface exchange are tabulated for the different mixture parameters. For the two parallel surfaces A_1 and A_2, a constant mean beam length is sufficient to correlate all the total geometric mean absorption and emission data. It is

$$L_{ma,12} = L_{me,12} = 1.16X \tag{16}$$

For the surface–surface radiative exchange between two perpendicular surfaces A_1 and A_3 and the surface–volume radiative exchange to surface A_1, numerical data show that it is sufficient to treat the mean beam lengths as functions of only the total absorption partial pressure (P_g) and soot volume fraction (f_v). The average emission and absorption mean beam lengths (averaging over the mixture temperature and composition) for the surface–surface exchange ($L_{me,13}$ and $L_{ma,13}$) and surface–volume exchange ($L_{me,1}$ and $L_{ma,1}$) are plotted as a function of the total pressure pathlength and different volume fraction pathlengths in Figs. 2a and 2b. The total geometric mean absorptance and emittance generated by the average mean beam length are plotted against the exact numerical data in Figs. 3a and 3b. It can be readily observed that while the mixture temperature (T_g) and CO_2 fraction (F_{CO_2}) have some effect on the mean beam length (as seen in Figs. 2a and 2b), the average geometric mean absorptance and emittance are in excellent agreement with the numerical data. Treating these mean beam lengths as functions of two parameters (P_gX and f_vX), they can be readily correlated by a simple three-layer neural network (MBL-NNET) as follow

$$a^3 = \sum_{i=1}^{S_3} a_i^2 W_i^3 + b^3 \tag{17}$$

with

$$a_i^2 = \tanh\left[\left(\sum_{j=1}^{S_1} W_{ij}^2 a_j^1\right) + b_i^2\right], \quad i = 1, \ldots, S_2 \tag{18}$$

$$a_i^1 = \tanh\left[\left(\sum_{j=1}^{2} W_{ij}^1 p_j\right) + b_i^1\right], \quad i = 1, \ldots, S_1 \tag{19}$$

In the above expressions, a^3 is the correlated mean beam lengths ($L_{me,13}$, $L_{ma,13}$, $L_{me,1}$, $L_{ma,1}$), and p_j is the input parameters with

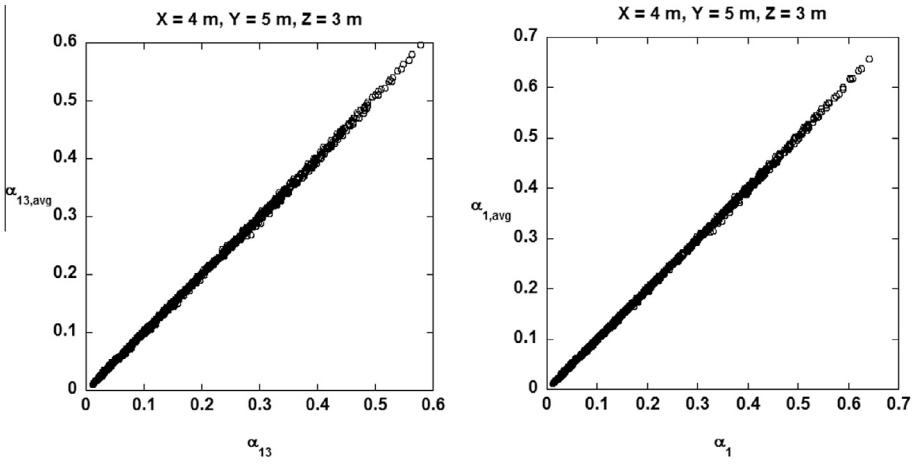

Fig. 3a. Comparison between the average total absorptances (generated by the average mean beam length) with the exact numerical data over all range of the system parameters ($0 < P_gX < 100$ kPa m, $0 < f_vX < 3 \times 10^{-7}$ m, $300 < T_g < 2000$ K, $0 < F_{CO_2} < 1$, $T_w = 1000$ K).

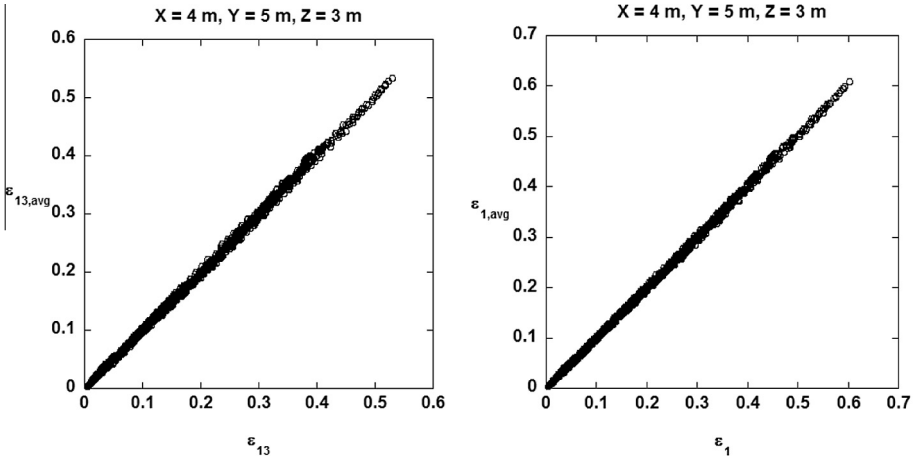

Fig. 3b. Comparison between the average total emittances (generated by the average mean beam length) with the exact numerical data over all range of the system parameters ($0 < P_gX < 100$ kPa m, $0 < f_vX < 3 \times 10^{-7}$ m, $300 < T_g < 2000$ K, $0 < F_{CO_2} < 1$).

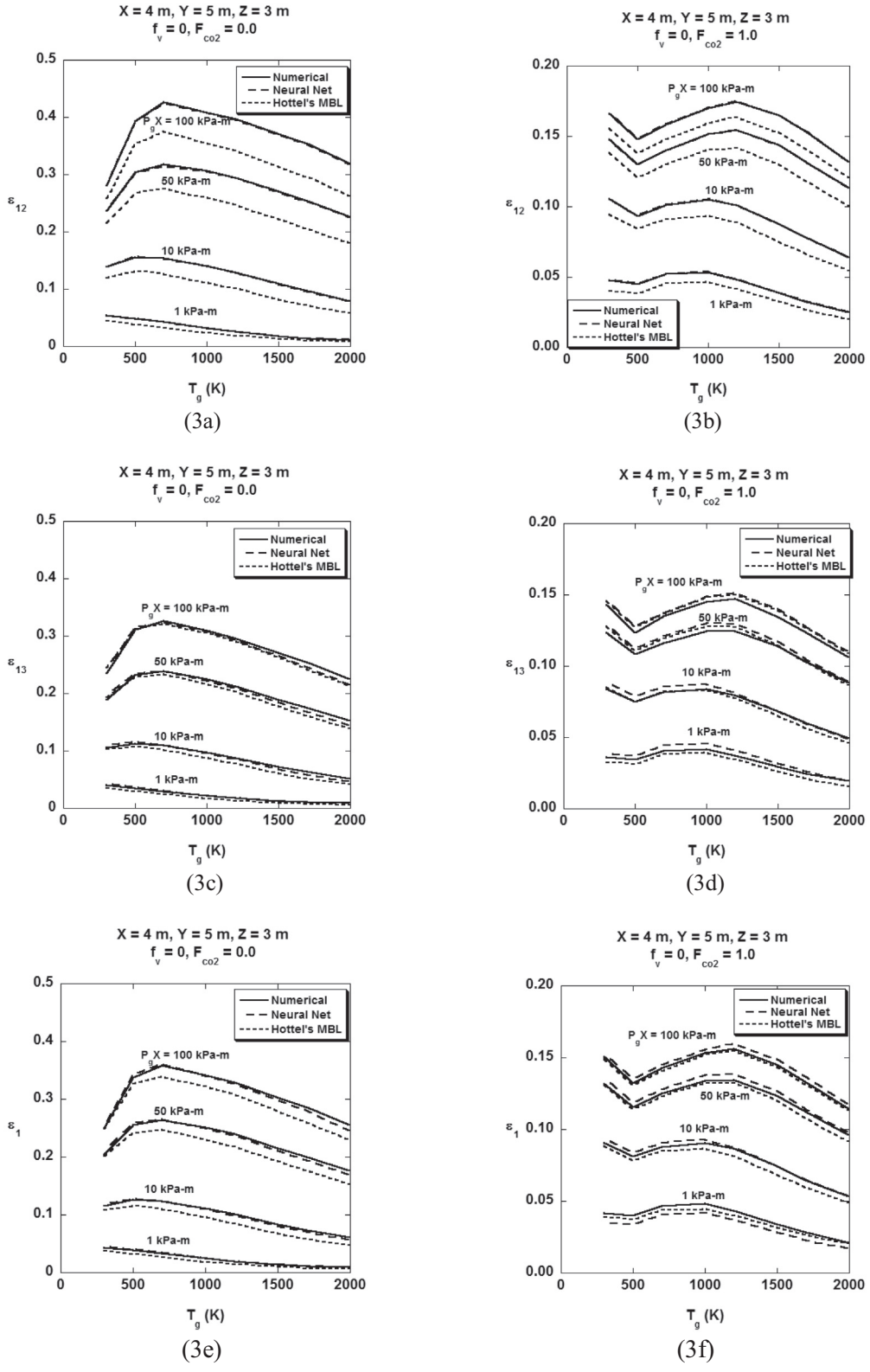

Fig. 4. Geometric mean emittances (ε_{12}, ε_{13}, ε_1) for a pure H_2O gas (3a, 3c, 3e) and a pure CO_2 gas (3b, 3d, 3f) at different pressure pathlength (P_gX) and gas temperature (T_g) generate by the three approaches (direct numerical integration, neural network and Hottel's MBL).

$p_1 = P_gX$ and $p_2 = f_vX$. The numerical values of the correlated parameters S_1, S_2, W_{ij}, b_i^1, b_i^2 and b^3 are available upon request. The neural network can predict the numerical data to within a relative accuracy of 5%.

3.2. The total geometric mean absorptance and emittance

In this section, the total geometric mean absorptance and emittance generated by RAD-NNET and MBL-NNET are computed and

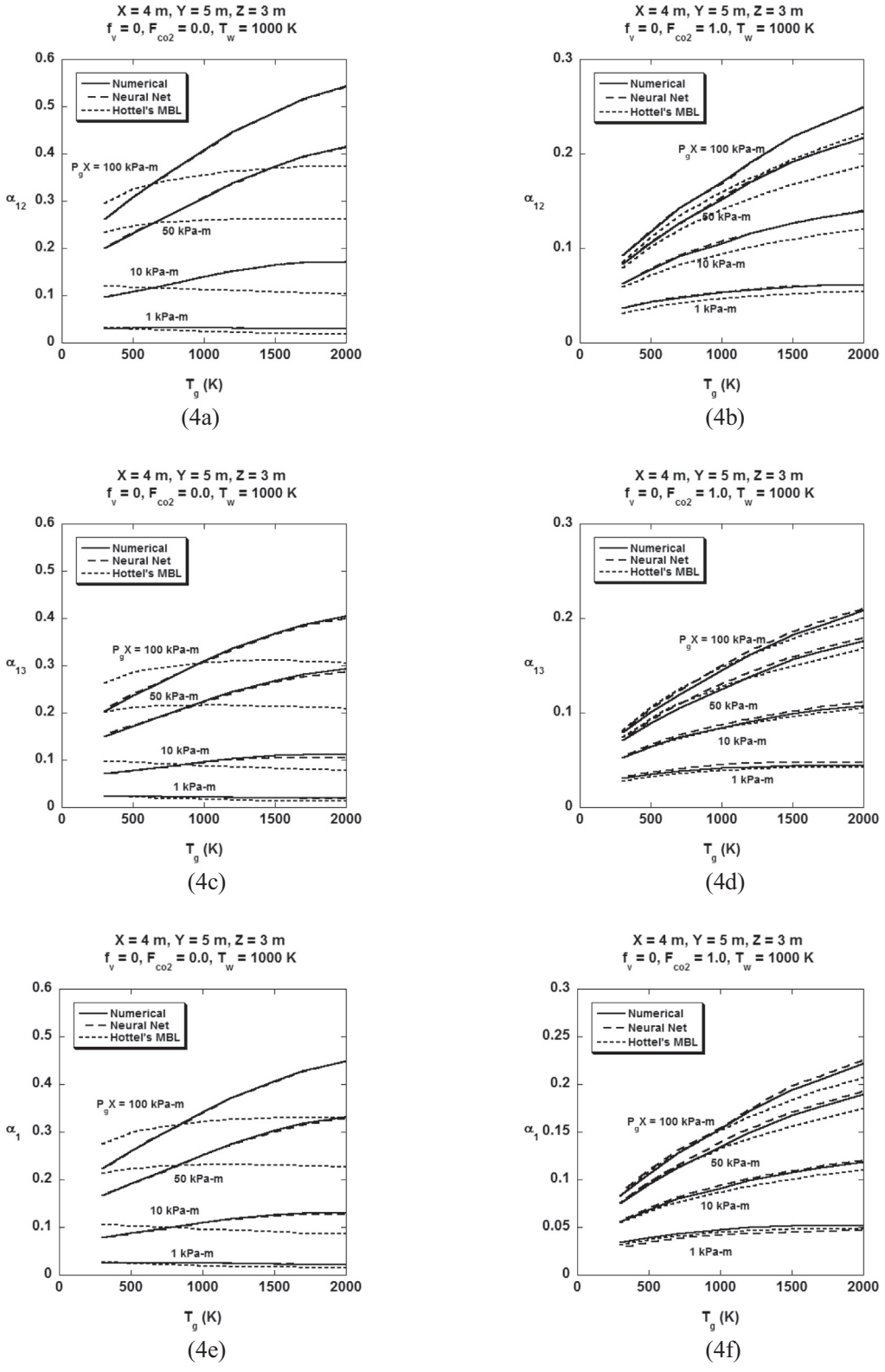

Fig. 5. Geometric mean absorptances (α_{12}, α_{13}, α_1) for a pure H_2O gas (4a, 4c, 4e) and a pure CO_2 gas (4b, 4d, 4f) at different pressure pathlength (P_gX) and gas temperature (T_g) generate by the three approaches (direct numerical integration, neural network and Hottel's MBL).

compared with the exact numerical results. In addition, results generated by the Hottel's mean beam length approach are also generated and compared with the numerical solution. Specifically, in the constant mean beam length approach recommended by Hottel [1], the emittance of a general $N_2/CO_2/H_2O$ mixture is generated from the emittance of the individual component by the following expression

$$\varepsilon_i(T_g, P_gX, F_{CO_2}) = \varepsilon_{1D,H_2O}(T_g, P_{H_2O}L_{m,c}) + \varepsilon_{1D,CO_2}(T_g, P_{CO_2}L_{m,c}) - \Delta\varepsilon \tag{20}$$

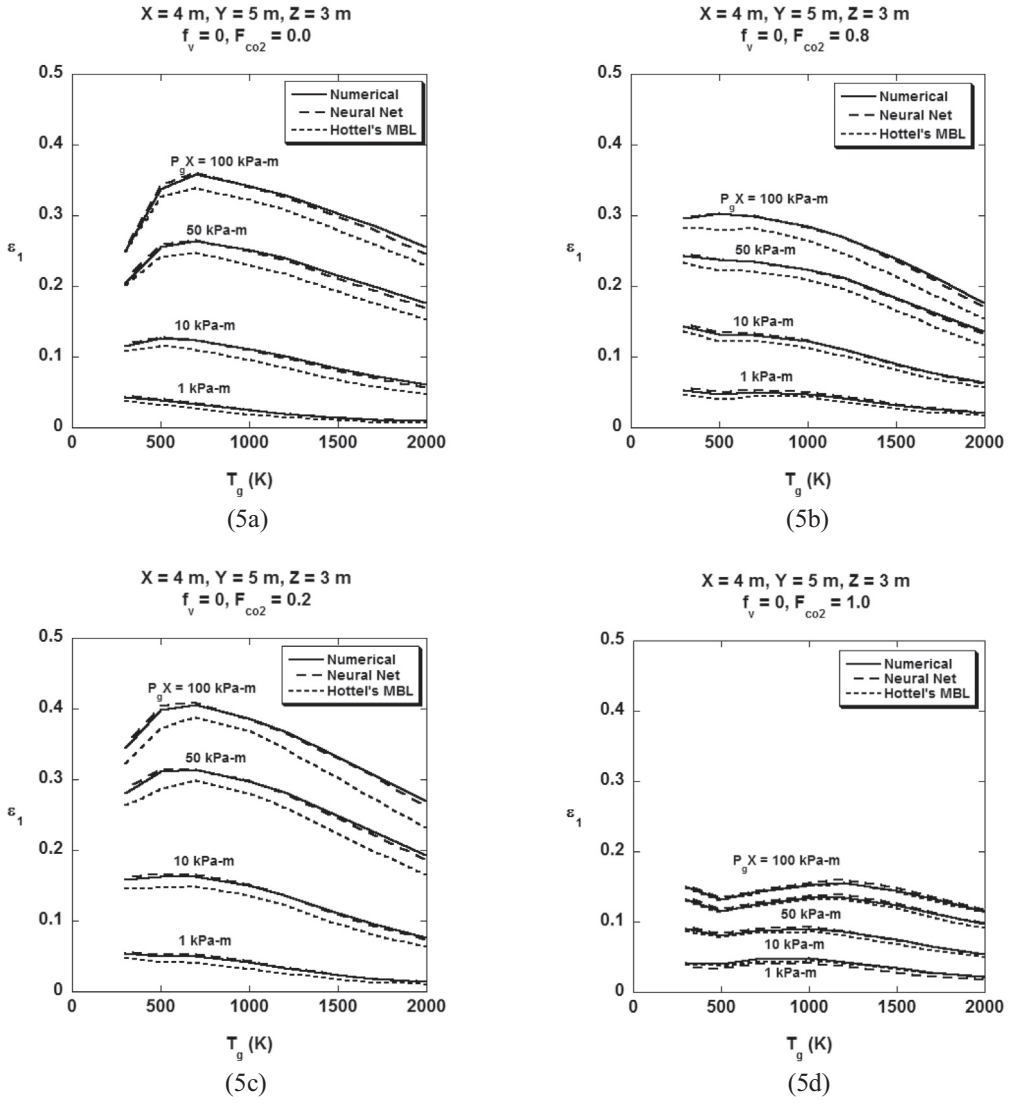

Fig. 6. Geometric mean emittances from the mixture volume to surface A_1 (ε_1) for a non-luminous H_2O/CO_2 gas mixture with different composition at different pressure pathlength (P_gX) and gas temperature (T_g) generate by the three approaches (direct numerical integration, neural network and Hottel's MBL).

with ε_{1D} being the one-dimensional emittance with a mean beam length of

$$L_{m,c} = 3.6\frac{V}{A} \tag{21}$$

where V and A is interpreted as the volume of the mixture enclosed by the considered surfaces under consideration. The emittance for CO_2 and H_2O are presented in graphical form known as the Hottel's emissivity chart. These charts, together with the correction factor $\Delta\varepsilon$, are given in Ref. [1]. For the absorptance, the recommended approach [1] is to use an expression similar to that of Eq. (20) given by

$$\alpha_i(T_w, T_g, P_gX, F_{CO_2}) = \alpha_{1D,H_2O}(T_w, T_g, P_{H_2O}L_{m,c}) + \alpha_{1D,CO_2}(T_w, T_g, P_{CO_2}L_{m,c}) - \Delta\alpha \tag{22}$$

with

$$\alpha_{1D,H_2O}(T_w, T_g, P_{H_2O}L_{m,c}) = C_{H_2O}\left(\frac{T_g}{T_w}\right)^{0.45} \times \varepsilon_{1D,H_2O}\left(T_g, P_{H_2O}L_{m,c}\frac{T_g}{T_w}\right) \tag{23a}$$

$$\alpha_{1D,CO_2}(T_w, T_g, P_{CO_2}L_{m,c}) = C_{CO_2}\left(\frac{T_g}{T_w}\right)^{0.65} \times \varepsilon_{1D,CO_2}\left(T_g, P_{CO_2}L_{m,c}\frac{T_g}{T_w}\right) \tag{23b}$$

and

$$\Delta\alpha = \Delta\varepsilon(T_g) \tag{23c}$$

The two empirical constants C_{H_2O} and C_{CO_2} are also provided graphically in Ref. [1].

Numerical data for the total geometric mean emittances (ε_{12}, ε_{13} and ε_1) for a non-luminous ($f_v = 0$) mixtures with a single absorption gas (N_2/H_2O or N_2/CO_2) generated by the three approaches (numerical, neural net and Hottel's MBL) are presented in Fig. 4 and the corresponding data for the total geometric mean absorptances (α_{12}, α_{13} and α_1) are shown in Fig. 5. To illustrate the relative accuracy for the neural network approach and the Hottel's mean beam length approach for a non-luminous gas mixture with two absorption gases, the volume–surface total geometric mean emittance and absorptance (ε_1 and α_1) for various mixture proportion (F_{CO_2}) are presented in Figs. 6 and 7. For simplicity, in the evaluation of the 1-D emittances and absorptances using the

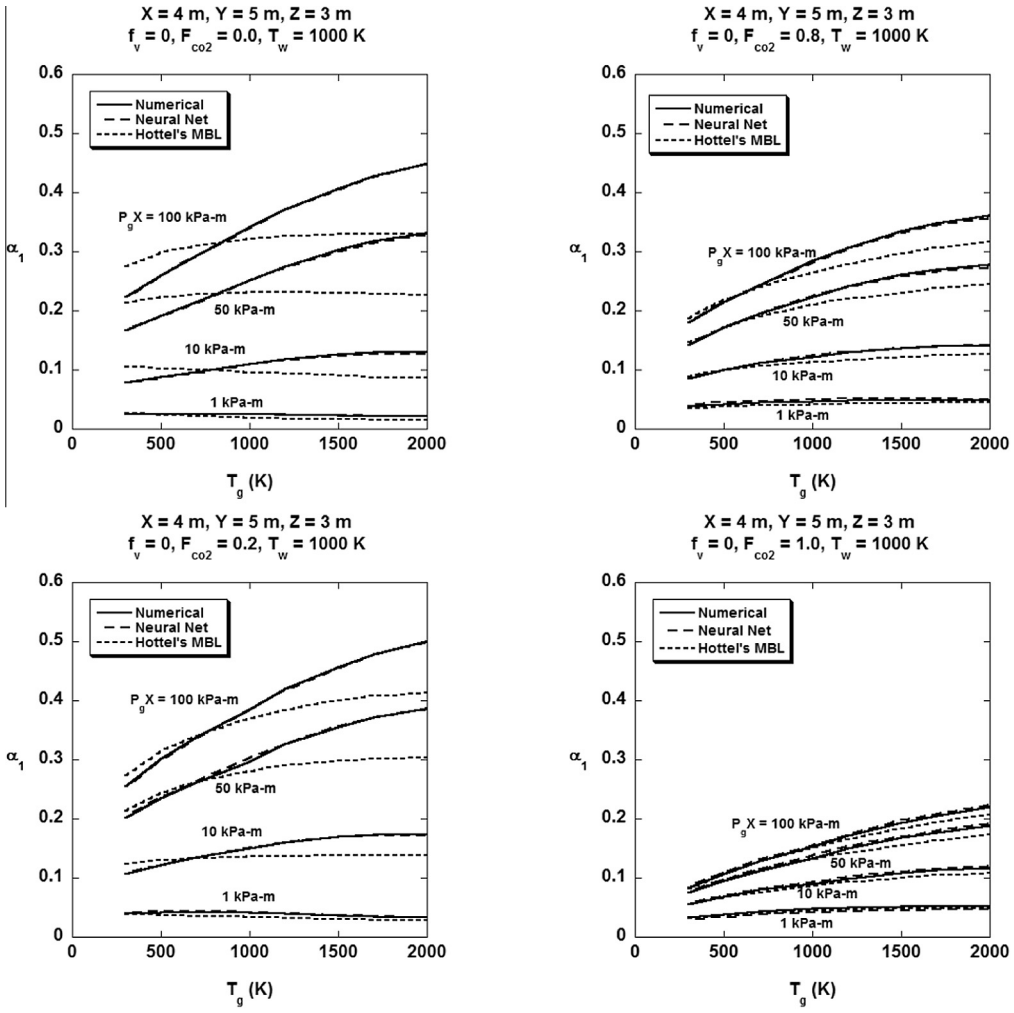

Fig. 7. Geometric mean absorptances from the mixture volume to surface A_1 (α_1) for a non-luminous H_2O/CO_2 gas mixture with different composition at different pressure pathlength (P_gX) and gas temperature (T_g) generate by the three approaches (direct numerical integration, neural network and Hottel's MBL).

Hotel's MBL and Eqs. (20) and (23), RAD-NNET is used instead of the Hottel's emittance chart. Finally, for a luminous mixture with non-zero soot volume fraction, the volume–surface total geometric mean emittance and absorptance for a $N_2/H_2O/CO_2$/soot mixture with $F_{CO_2} = 0.8$ and different soot volume fraction are presented in Figs. 8 and 9. Since the Hottel's MBL approach is not applicable for a luminous mixture, the accuracy of the additive approach (addition of a pure soot solution with a pure gas solution) is evaluated in these figures.

With regard to the numerical accuracy of the neural network approach and the Hottel's MBL approach, the following conclusions can be made from the data presented in Figs. 4–9:

1. The neural network approach using RAD-NNET and MBL-NNET is uniformly accurate over the entire range of the mixture parameters (Figs. 4–9).
2. The Hottel's MBL approach is reasonably accurate in predicting the total geometric mean emittance except for the surface–surface total geometric mean emittance between surfaces A_1 and A_2, ε_{12} (Figs. 4 and 6).
3. The Hottel's MBL approach is generally inaccurate in predicting the total geometric mean absorptance, particularly for mixture with a high percentage of H_2O. It fails to predict neither magnitude of the absorptance nor the trend of increasing absorptance with mixture temperature. The improved accuracy of the Hottel's MBL approach for a mixture with large CO_2 concentration is probably due to the matching of the 2.7 μm absorption band with the peak of the Planck function at the emission temperature of 1000 K (~3 μm) (Figs. 5 and 7). This improvement in accuracy is not expected for other emission temperatures.
4. The additive solution is not a viable approximation for the prediction of absorptance and emittance of a luminous gas mixture, except in the limit of small soot volume fraction (Figs. 8 and 9).

With regard to the physics of absorption and emission for a three-dimensional nongray mixture, the following conclusions can be made from the data presented in Figs. 4–9:

1. The general gray assumption of emittance equal to absorptance is uniformly invalid over all range of the mixture properties (Figs. 4–9).
2. The combined effect of CO_2 and H_2O on the mixture absorption/emission is a highly nonlinear function of the mixture fraction of the individual component due to the much stronger absorption effect by H_2O as compared to CO_2. A 20% CO_2 mixture fraction ($F_{CO_2} = 0.2$) leads to only a slight increase in the total geometric absorptance and emittance compared to the pure H_2O case ($F_{CO_2} = 0$). A 20% H_2O mixture fraction ($F_{CO_2} = 0.8$),

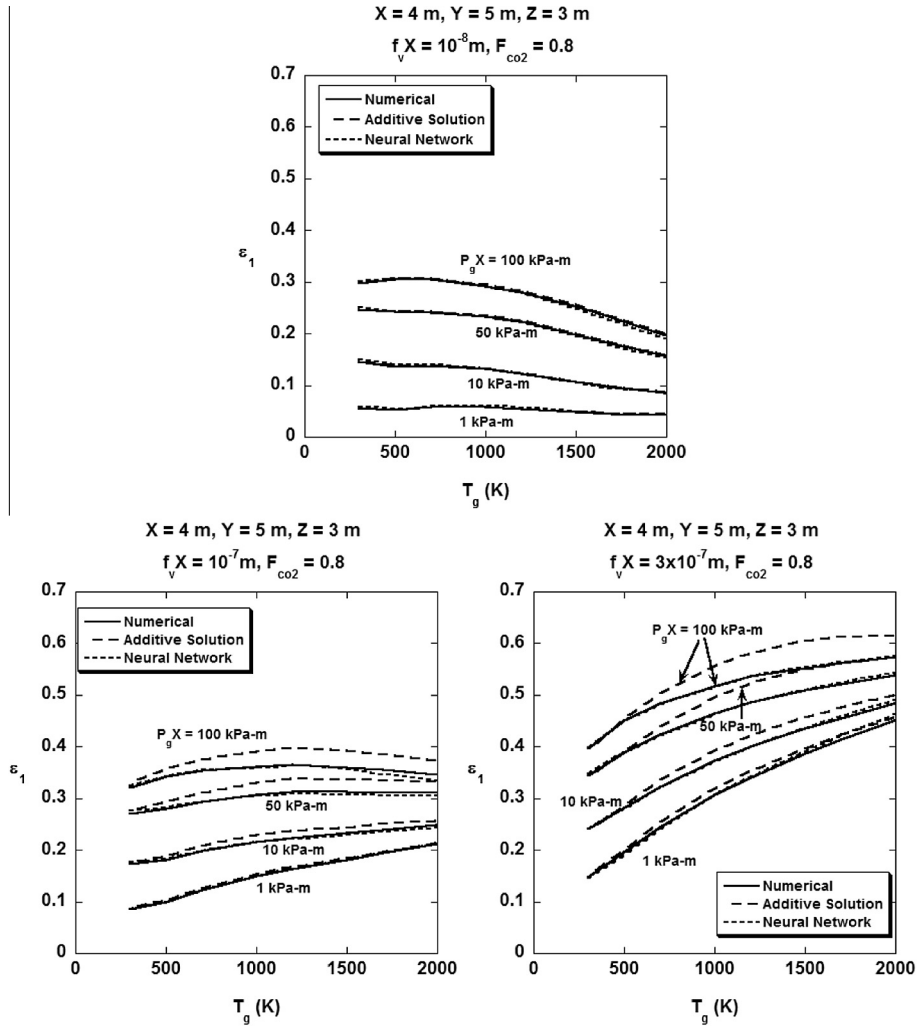

Fig. 8. Geometric mean emittances from the mixture volume to surface A_1 (ε_1) for a luminous H_2O/CO_2 gas mixture with a fixed composition ($F_{CO_2} = 0.8$) and different soot volume fraction at different pressure pathlength (P_gX) and gas temperature (T_g) generate by the three approaches (direct numerical integration, neural network and additive solution).

on the other hand, leads a significant increase in the total geometric absorptance and emittance compared to the pure CO_2 case ($F_{CO_2} = 1.0$) (Figs. 6 and 7).

3. The mixture temperature generally has a different effect on its emittance and absorptance. In general, the mixture absorptance is a monotonically increasing function with the mixture temperature (Figs. 5, 7 and 9), while the mixture emittance can be an increasing or decreasing function with mixture temperature at different temperature regions (Figs. 4, 6 and 8). Indeed, for a luminous mixture, the mixture emittance changes from a decreasing function with mixture temperature when the soot concentration is low ($f_vX = 10^{-8}$ m) to an increasing function with mixture temperature when the soot concentration is high ($f_vX = 3 \times 10^{-7}$ m) (Fig. 8).

4. Conclusion

The mean beam length concept is demonstrated to be an effective concept to provide a simple, efficient and accurate approach to compute radiative heat transfer in non-gray three-dimensional mixtures. For a $N_2/CO_2/H_2O$/soot mixture at one atmosphere, different mean beam lengths are defined for the mixture's emittance and absorptance. These mean beam lengths are shown to depend strongly on the mixture total absorption pressure pathlength and soot volume fraction. While the mixture temperature and gas composition have some minor effect on the mean beam length, a mean beam length averaged over the mixture temperature and gas composition is sufficient to correlate the numerical data of the total absorptance and emittance. A neural network, MBL-NNET, is generated to correlate the numerical data of the mean beam length over the range of the mixture parameters. Together with RAD-NNET, the two neural networks provide an efficient and accurate approach to determine the absorption and emission characteristics for the three-dimensional non-gray mixture.

Even though the current work focuses on a rectangular enclosure with a specific dimension, the current approach can be readily adapted to enclosures with different geometries and mixtures involving other gaseous species (e.g. CO, CH_4, etc.) for which one dimensional gaseous absorption data are available. By investing some computational effort to generate the necessary neural networks (which is quite viable with the computational power currently available even for notebook computers), RAD-NNET and MBL-NNET can be made available for a specific three-dimensional enclosure and gas/soot mixture to provide an accurate simulation of the radiation heat transfer effect for application in transient engineering design calculations.

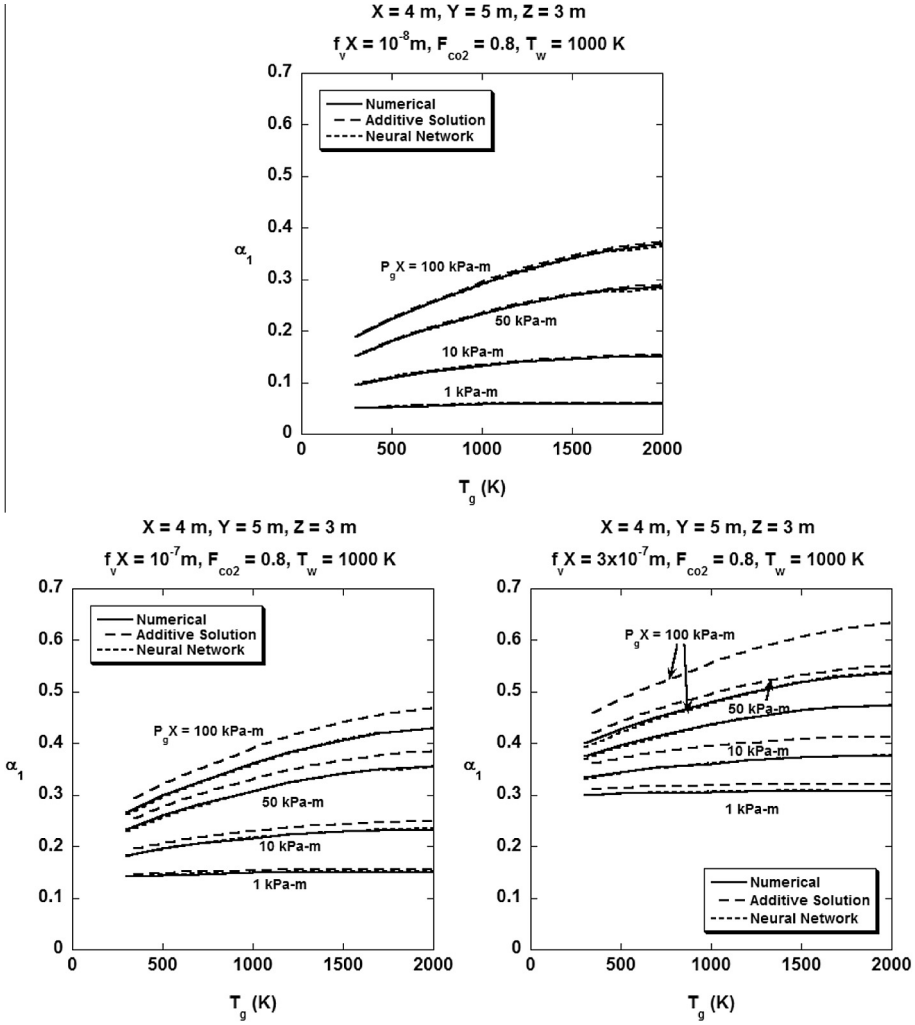

Fig. 9. Geometric mean absorptances from the mixture volume to surface A_1 (α_1) for a luminous H_2O/CO_2 gas mixture with a fixed composition ($F_{CO_2} = 0.8$) and different soot volume fraction at different pressure pathlength (P_gX) and gas temperature (T_g) generate by the three approaches (direct numerical integration, neural network and additive solution).

Conflict of interest

None declared.

References

[1] H.C. Hottel, Chapter 4, radiant-heat transmission, in: W.H. MacAdams (Ed.), Hear Transmission, McGraw-Hill, New York, 1954.
[2] A.K. Oppenheim, J.T. Bevans, Geometric factor for radiative heat transfer through an absorbing medium in Cartesian co-ordinates, ASME J. Heat Transfer 82 (4) (1960) 360–368.
[3] D.B. Olfe, Mean beam length calculations for radiation from non-transparent gases, J. Quant. Spectrosc. Radiat. Transfer 1 (1961) l69–176.
[4] R.V. Dunkle, Geometric mean beam length for radiant heat transfer calculations, ASME J. Heat Transfer 86 (1) (1964) 74–80.
[5] C.L. Tien, L.S. Wang, On the calculation of mean beam length for a radiating gas, J. Quant. Spectrosc. Radiat. Transfer 5 (1965) 453–456.
[6] D.A. Mandell, F.A. Miller, Comparison of exact and mean beam length results for a radiating hydrogen plasma, J. Quant. Spectrosc. Radiat. Transfer 13 (1973) 49–56.
[7] W.W. Yuen, Development of a network analogy and evaluation of mean beam lengths for multi-dimensional absorbing/isotropically scattering media, ASME J. Heat Transfer 112 (1990) 408–413.
[8] W.W. Yuen, A. Ma, Evaluation of total emittance of an isothermal nongray absorbing, scattering gas-particle mixture based on the concept of absorption mean beam length, ASME J. Heat Transfer 114 (1992) 653–658.
[9] M. Schoenwetter, D. Vortmeyer, A new model for radiation heat transfer in emitting, absorbing and anisotropically scattering media based on the concept of mean beam length, Int. J. Therm. Sci. 39 (2000) 983–990.
[10] P. Cheng, Exact solution and differential approximation for multi-dimensional radiative transfer in cartesian coordinate configuration, Prog. Astronaut. Aeronaut. 31 (1972) 269.
[11] K.Y. Wang, C.L. Tien, Radiative heat transfer through opacified fibers and powders, J. Quant. Spectrosc. Radiat. Transfer 30 (3) (1983) 213–223.
[12] H.C. Hottel, A.F. Sarofim, Radiative Transfer, McGraw Hill, New York, 1967.
[13] G.D. Raithby, E.H. Chui, A finite-volume method for predicting a radiant heat transfer in enclosures with participating media, J. Heat Transfer 112 (1990) 415–423.
[14] W.A. Fiveland, Discrete ordinate method for radiative transfer in isotropically and anisotropically scattering media, J. Heat Transfer 109 (3) (1987) 809–812.
[15] J.R. Howell, M. Perlmutter, Monte Carlo solution of thermal transfer through radiant media between gray walls, ASME J. Heat Transfer 86 (1) (1964) 116–122.
[16] M. Modest, The weighted-sum-of-gray-gas model for arbitrary solution methods in radiative transfer, ASME J. Heat Transfer 113 (3) (1991) 650–656.
[17] K. McGrattan, R. McDermott, C. Weinschenk, K. Overholt, S. Hostikka, J. Floyd, Fire dynamics simulator technical reference guide volume 1: mathematical model, in: NIST Special Publication 1018, sixth ed., NIST, 2014.
[18] FLUENT 6.1 User's Guide, Fluent, Inc. 2003.
[19] F.P. Incropera, D.P. DeWitt, Introduction to Heat Transfer, sixth ed., John Wiley and Son, 2011.
[20] J.P. Holman, Heat Transfer, 10th ed., McGraw Hill, 2010.
[21] R. Siegel, J. Howell, Thermal Radiation Heat Transfer, fourth ed., Taylor and Francis, New York, 2002.
[22] M.F. Modest, Radiative Heat Transfer, second ed., Academic Press, 2003.
[23] W.W. Yuen, RAD-NNET, a neural network based correlation developed for a realistic simulation of the non-gray radiative heat transfer effect in three-dimensional gas-particle mixture, Int. J. Heat Mass Transfer 52 (2009) 3159–3168.
[24] W.L. Grosshandler, RADCAL, A Narrow-Band Model for Radiation Calculations in a Combustion Environment, NIST-TN-1402, National Institute of Standard and Technology, April 1993.